Landslides (2020) 17:191–204
DOI 10.1007/s10346-019-01309-1
Received: 30 June 2019
Accepted: 24 October 2019
Published online: 15 November 2019

Zhuo Chen · Danqing Song · Chao Hu · Yutian Ke

The September 16, 2017, Linjiabang landslide in Wanyuan County, China: preliminary investigation and emergency mitigation

Abstract This paper reports on a typical slow-moving landslide that occurred in Shuitianba village in Wanyuan County, Sichuan Province, China, on September 16, 2017. The landslide in Wanyuan County is regionally outstanding for its features and well-developed landslide morphology. Hence, this event can provide a good case study for understanding the possible triggering conditions of the occurrences of all the landslides examined in Wanyuan County. The 225 residents of Shuitianba village did not flee the village because the deformation of the landslide was extremely slow. However, the primary emergency tasks are still necessary to reduce the landslide risk that may affect the residents. Detailed field investigations, boreholes, and exploratory trenches were performed to investigate the characteristics and triggering factors of this landslide. Rainfall and anthropogenic activities (such as informal, unplanned settlements and deforestation) were revealed to be the main triggering factors. The main engineering control measures, including anti-sliding piles, an anti-sliding retaining wall, and intercepting ditch, were applied to stabilize the landslide. However, landslide mitigation measures have not been finished, and hence, some interim measures are suggested to effectively reduce landslide risk.

Keywords Landslide · Landslide features · Emergency mitigation · Wanyuan County · China

Introduction

Landslides are widely distributed in Southwest China and became a major risk to human life and property (Xu et al. 2014; Ma et al. 2018; Song et al. 2018; Ma et al. 2019). Wanyuan County is one of the regions that is heavily affected by landslide disasters in northeast Sichuan Province, China. A total of 321 active landslides were registered in this region, and landslide occurrence has increased markedly since the 1980s according to records.

Although landslides occur frequently in remote mountainous areas, they still receive increased attention from many scholars (Shirzadi et al. 2017; Samodra et al. 2018; Hu et al. 2019). Many landslide cases have been reported and posed important engineering problems (Gischig et al. 2016; Wang et al. 2016; Yerro et al. 2016). Generally, landslides can be initiated not only by natural causes, including earthquakes and intense or prolonged rainfall but also by anthropogenic activities such as road construction or house overloading (Lin et al. 2018; Ma et al. 2018). The expanding population and buildings bring human habitation within reach of potential landslide hazards. The number of people living in the loose mixed deposits of Southwest China has significantly increased the possibility of landslide occurrence. The Linjiabang landslide is a typical slow-moving landslide and is also regionally outstanding for its features and well-developed landslide morphology. This landslide can provide a good reference for triggering conditions in Wanyuan County.

Understanding the causes and conditions of a landslide disaster is important to landslide prevention and to providing useful information for engineers choosing landslide mitigation measures (Đurić et al. 2017; Luo et al. 2017; Song et al. 2019; Huang et al. 2019). According to previous geological experience, if effective engineering measures were not implemented to control the continuous displacement of the landslide, the landslide would pose a serious threat to the safety of human life and property. Furthermore, the 225 residents of Shuitianba village did not flee the village due to the extremely slow deformation of the landslide. To reduce the landslide risk, ground investigations, mapping, boreholes, exploratory trenches, and emergency mitigation have been conducted since October 2017. This paper describes the landslide characteristics and possible triggering conditions and discusses landslide mitigation measures.

Study area

The landslide occurred in Shuitianba village in Wanyuan County, Sichuan Province (Figs. 1 and 2). Shuitianba village is situated in the northeastern sector of Sichuan Province, on the southeast limb of the Shiziba anticlinorium. It is located approximately 541 km from Chengdu, the capital of Sichuan Province. The study area is located in the transition zone between the Tibetan Plateau and the Sichuan Basin, and its topography includes low–middle mountains and hills. Through field investigation, the bedrock exposed in the region is the Middle Triassic Badong Formation (T_2b), which consists of pelitic limestone intercalated with thin mudstone. A mantle of Quaternary deposits overlies the Badong Formation, and the deposits mainly consist of residual and diluvial deposits as well as reworked landslide deposits. According to the Dazhou Meteorological Bureau (http://www.dzjzw.com/) in Sichuan Province, this area belongs to a subtropical monsoon climate with a mean annual temperature of 14.7 °C. The annual average rainfall from 1985 to 2017 is 1232.7 mm, with a minimum of 771.2 mm in 1962 and a maximum of 2218 mm in 1988. The rainfall mainly concentrates in June to September and accounts for 65.94% of the annual rainfall.

Landslide features

The Linjiabang landslide (32°9′48.96″N, 108°1′25.36″E) is approximately 200 m in length and 240 m in width, with a mean depth of 15 m (Fig. 3). The estimated area of the landslide body is 4.8×10^4 m^2, the volume is approximately 7.2×10^5 m^3, the main sliding direction is approximately 207°, the elevation ranges from 776 to 845 m, the height difference is 69 m, and the average gradient is 16°. The major road in this area traverses the middle and rear section of the landslide.

A significant number of tension cracks, minor scarps and bulges have been found on the landslide surface (Fig. 4). Detailed

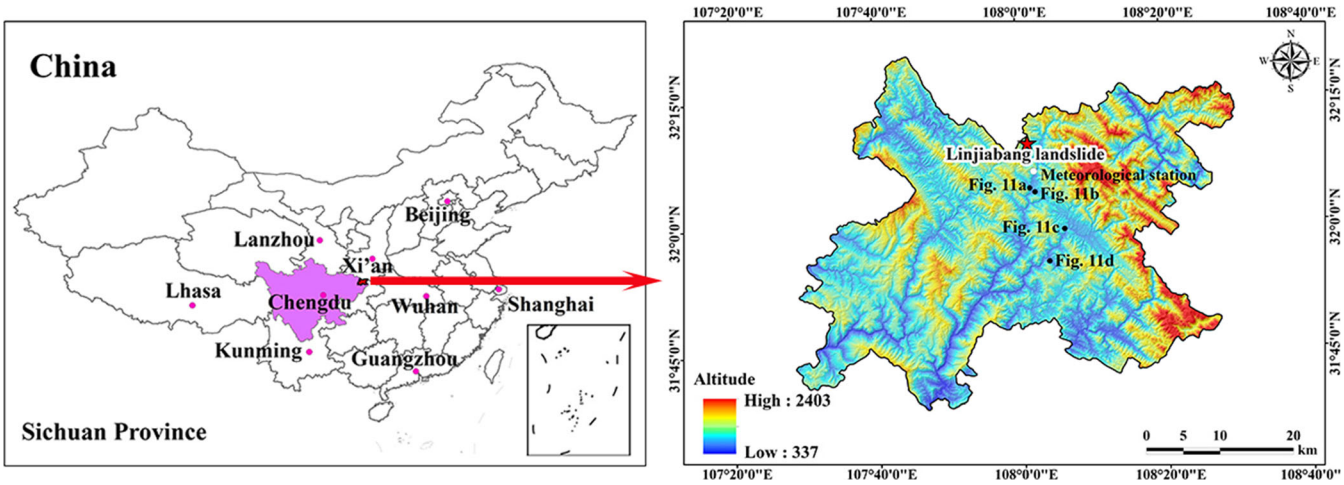

Fig. 1 Location of the landslide in Guandu Town, Wanyuan County, Sichuan Province, Southwest China

site investigations and inquiring local inhabitants revealed ten tension cracks developed gradually at the middle and rear region of the landslide. These cracks have lengths of 7–95 m, widths of 5–30 cm, observed depths of 10–50 cm, and vertical displacements of 10–60 cm. The cracks caused damage to some houses; moreover, two long continuous tension cracks developed along the concrete road at an elevation of 824 m.

Boreholes and exploratory trenches are used to investigate the geological structure of the landslide and potential slide surfaces. The locations of the boreholes and the exploratory trenches are shown in Fig. 3. The landslide structure, including silty clay, clay, and pelitic limestone, is shown in detail in Fig. 5. Based on the boreholes and the exploratory trenches, two slip surfaces S1 and S2 were found (Figs. 5 and 6). The upper slip surface is a secondary slip surface at a depth of 2.5 to 10.8 m, and the lower one is the entire slip surface along the interface between the bedrock and the overlying deposit at a depth of 10.3 to 18 m. The sliding zone is a continuous, 15- to 30-cm-thick zone. To obtain the shear strength parameters of the slide zone soil, the shear test was implemented with a direct shear apparatus. The friction angle and cohesion of the saturated sample were 8.5–9.7° and 18.1–19.4 kPa, respectively.

Based on topography and deformation characteristics, the Linjiabang landslide can be classified into two deformation areas: the rear strong deformation area and the front weak deformation area (Figs. 3, 6, 7, 8, 9, and 10). Abundant deformation (such as subsidence, tensile cracks, and bulges) could be observed in the rear strong deformation area. The elevation of the rear area varies from 804 to 845 m, the mean gradient is 20°, the extent is approximately 2.51×10^4 m^2 in area, the mean thickness is 17 m, and the estimated volume is 4.267×10^5 m^3. Expanded cracks developed in the rear of the landslide

Fig. 2 Panoramic photograph of the landslide

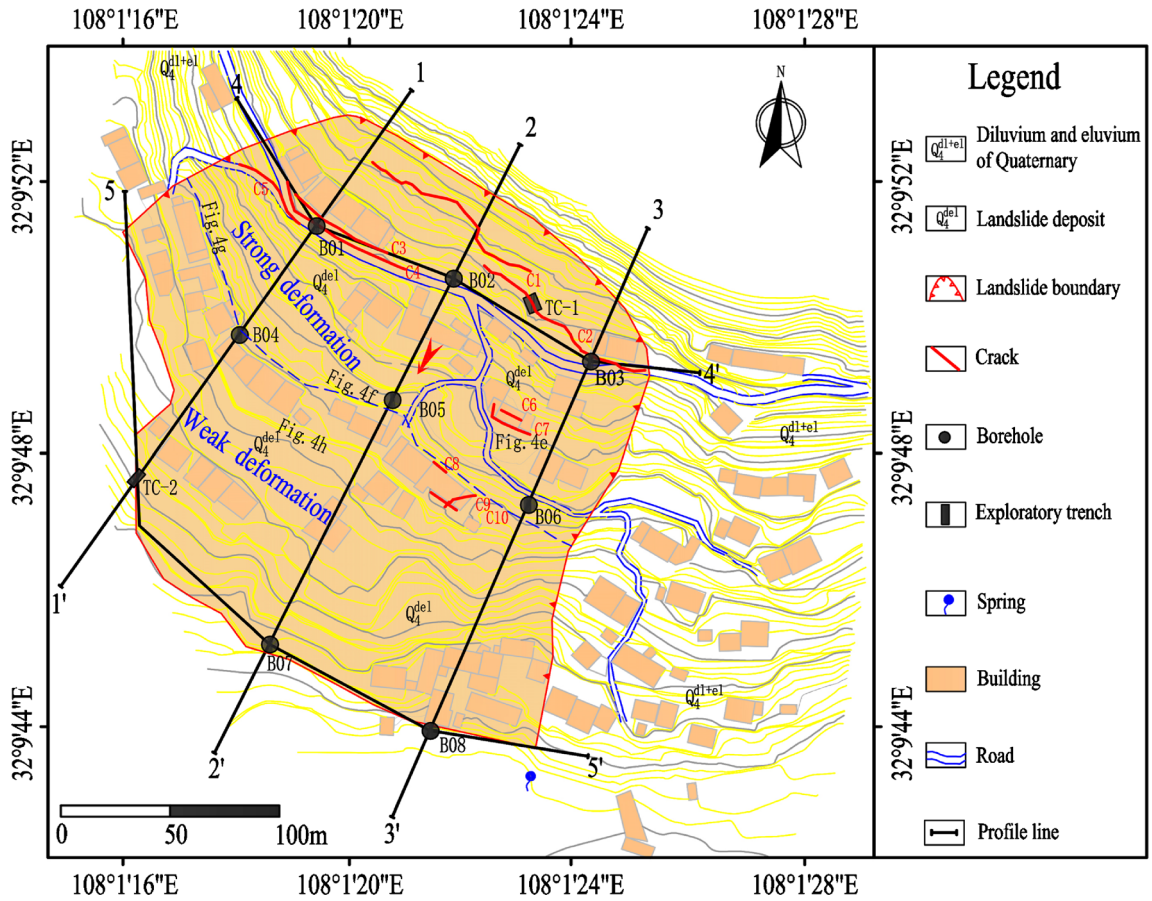

Fig. 3 Simplified engineering geological map of the landslide. The figure locations show the locations of Fig. 4

and several bulges in the mid-anterior. The front weak deformation area shows no obvious deformation features, but some tiny fissures were formed during the rainy season. This area has a mean thickness of 13 m, an area of 2.29×10^4 m^2, and an estimated volume of 2.933×10^5 m^3. The elevation of the front area ranges from 776 to 804 m, and the mean gradient is 12°.

Fig. 4 Cracks and bulges have been observed within the landslide body. **a** Crack C1. **b** Crack C2. **c** Crack C5. **d** Crack C9. The locations of bulges are shown in Fig. 3

Fig. 5 Lithological stratigraphic logs of boreholes (B02 and B05) and the slip zone of the Linjiabang landslide exposed by exploratory trench

Figures 6, 7, 8, 9, and 10 show the structure of the landslide material and the groundwater level in the landslide area. According to the stratum lithology and hydrogeologic conditions of this landslide, the groundwater in this area is mainly carbonatite karst water, which could be found in the contact zone between the bedrock and the overlying deposits. Groundwater is discharged to the ground surface in the form of a spring (Fig. 3). The spring on the southeast of the landslide yielded a flow of 0.1 l/s (6.0 l/min), which could be observed during the dry period every year.

In 1985, a local villager witnessed the slope slide in extremely low speed and found a crack on the rear part of the slope. However, the crack was filled with weathered materials. According to the information provided by local residents and field surveys, the Linjiabang landslide has undergone a long deformation history. Slow sliding was observed every year, especially during the rainy season, indicating a potentially highly dangerous area.

Triggering factors

Very high landslide potential in the future would endanger the lives and properties of local residents. Rainfall and anthropogenic activities (such as the informal, unplanned settlements, and deforestation) are responsible for the occurrence of the landslide.

Rainfall

During the rainy seasons of 2004–2005 and 2010–2011, rainfall events influenced most areas of Wanyuan County, causing landslides and floods (Fig. 11). The cumulative 2-day rainfall from 17 July to 19 July, 2010 totalled 450 mm. Notably, the temporal distribution of the landslides and the monthly mean rainfall presents high consistency (Fig. 12), and 87.45% of recorded landslide events occur between June and September. During the rainy period, more rain falls and may thus affect the occurrence and distribution of the landslides (Zhang and Huang 2018). Seasonal heavy rainfall could clearly influence the slope stability. However, the

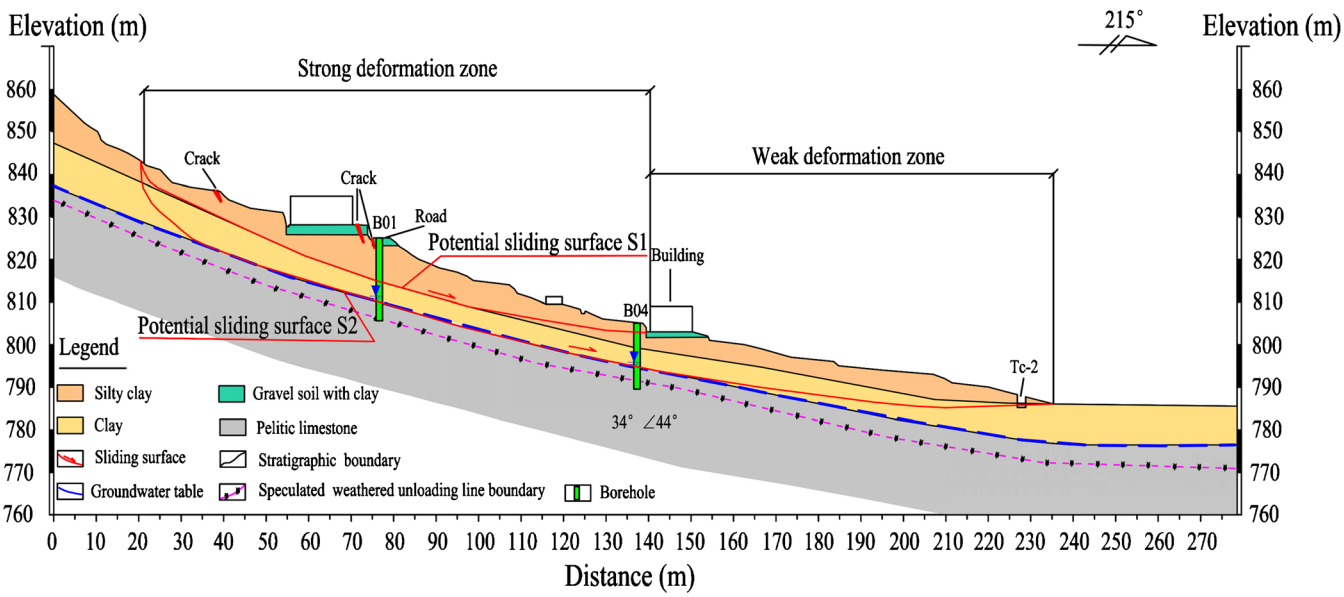

Fig. 6 Longitudinal geological profile 1-1′ (Fig. 3)

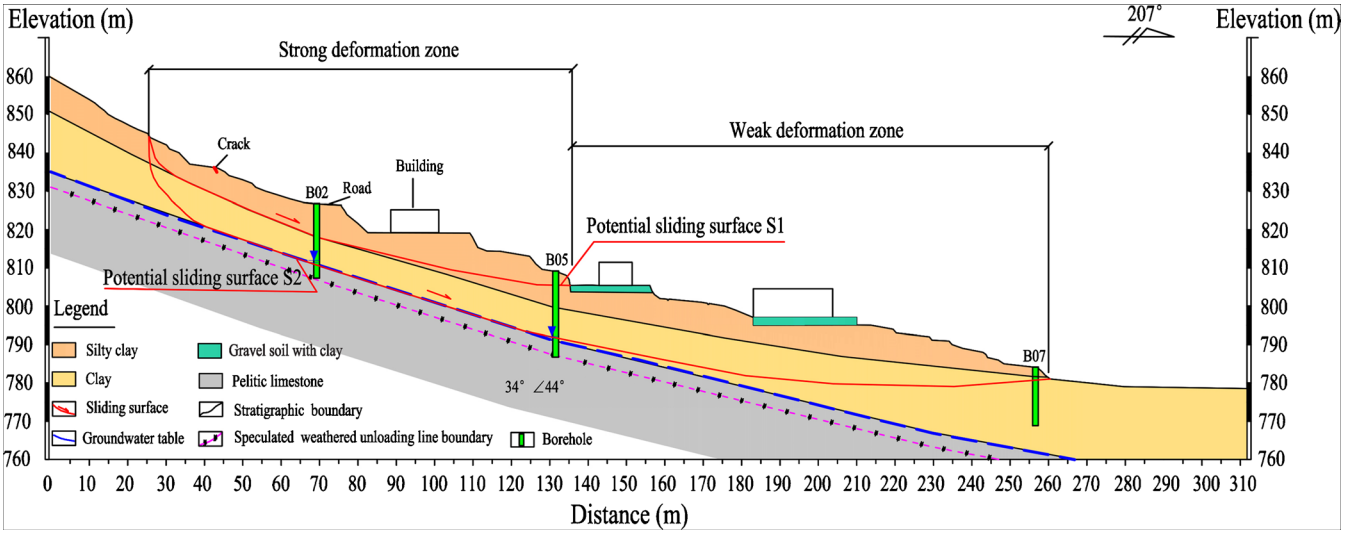

Fig. 7 Longitudinal geological profile 2-2′ (Fig. 3)

initiation of the studied landslide seems to be linked with longer-term trends rather than short-term heavy rainfall events. During rainfall, rainwater penetrated into newly formed cracks and reached the internal weak layers, markedly destabilizing the slope. Continuous rainfall may have saturated the sliding mass and increased the water content of the slip zone, leading to a major loss in the shear strength of the sliding zone. Hence, the stability of the slope approached the state of limit equilibrium. However, although long-term rain infiltration exists, the groundwater level still rises slightly because of the low permeability of the slope.

Anthropogenic activity

Anthropogenic activity, such as slope cutting for houses, land use changes, and deforestation, was also significant as a triggering factor for the Linjiabang landslide. Rapid urbanization in Wanyuan County contributed to the haphazard expansion of settlements. Figure 13 shows an increase from 11 houses in 1988 to 79 in 2019 in the landslide area, indicating insufficient risk management by the government. Shallow foundations were used in 79 houses with two to three floors. A considerable concentration of house overloading was acting on the slope, thereby further reducing the slope stability. Due to the high proportion of farmland (Fig. 13), irrigation demands in spring and summer may have an impact on the hydrological response of the slope and contribute to instability processes. The drainage ditch in the landslide area was built around the house and suffered severe deformation (Fig. 14). Inadequate drainage of surface water could have a negative effect on the slope stability. The slopes formerly occupied by arable lands are still liable to sliding even many years after abandonment. A comparison between the Google Earth© images in 2013 and 2017

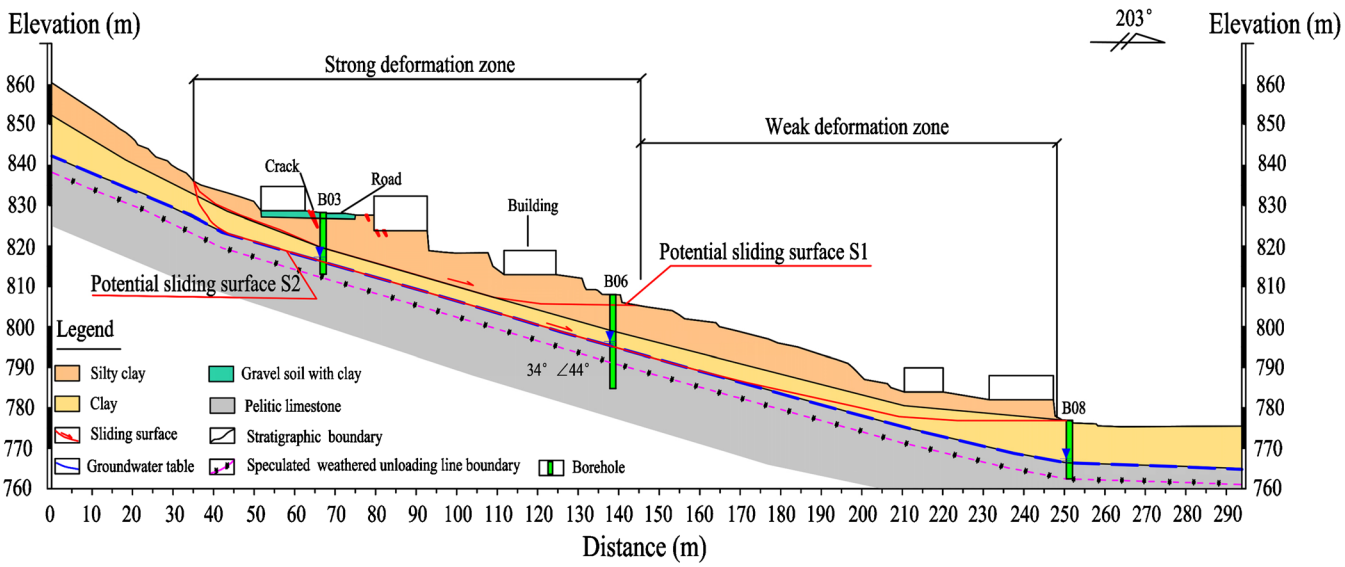

Fig. 8 Longitudinal geological profile 3-3′ (Fig. 3)

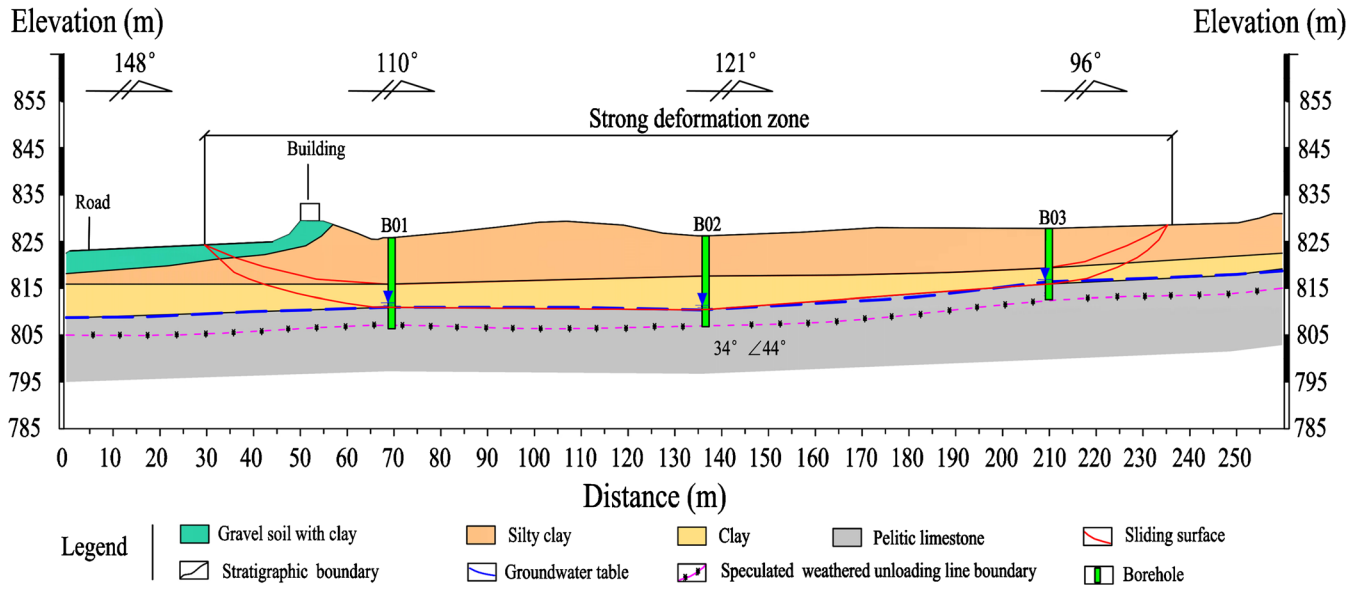

Fig. 9 Longitudinal geological profile 4-4′ (Fig. 3)

shows that the slope has undergone ecological damage due to deforestation (Fig. 15). Deforestation, such as cutting down trees and clearing land for crops, increases the seepage of rainwater into the ground, exerting a negative effect on slope stability.

Stability evaluation of the Linjiabang landslide

The stability evaluation of slopes has always received considerable attention from designers and constructors in geotechnical fields (Luo et al. 2017). In China, the limit equilibrium method (Bromhead 1992) is the most commonly used stability evaluation method because of its versatility and simple calculation process. However, when evaluating some special landslides (such as plastic flow, diffuse landslides, and lateral spreads), this method is not appropriate (Mendjel and Messast 2012). The important premises of this method involve three aspects: (i) the slip surface has been determined; (ii) the failure surface obeys the Mohr-Coulomb failure criterion; and (iii) the sliding mass is coherent during sliding.

The selection of appropriate geotechnical parameters is highly important for the accurate determination of slope stability. Through the direct shear tests, we can obtain the shear strength parameters of the slide zone soil. However, many factors (such as the heterogeneity of soil characteristics, the extraction of soil samples, and the handling and testing procedures) disturb the measurements of the shear strength parameters (Wei et al. 2012). Thus, it is difficult to obtain the appropriate parameters from testing. The back-calculation provides a relatively simple method to do this, especially when slopes exhibit on-going failure (Luo et al. 2017). The shear strength parameters obtained from the direct shear tests were good references for later back-calculation. The strength parameters of the slide zone soil were back-calculated by taking the safety factor (*Fs*) as 1.0. The back-calculation can be done with:

$$C = \frac{Fs\sum W_i \sin\alpha_i - \tan\phi \sum W_i \cos\alpha_i}{L} \quad (1)$$

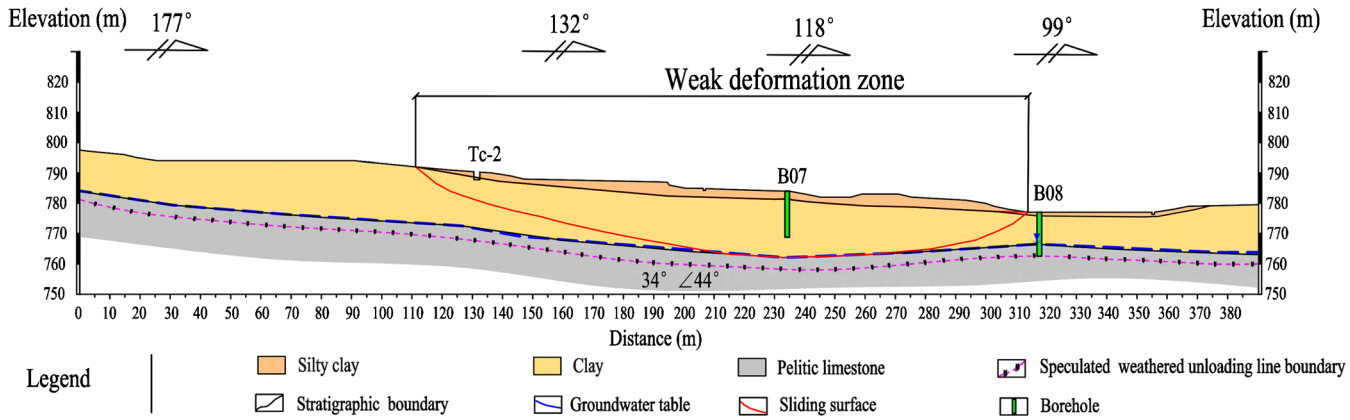

Fig. 10 Longitudinal geological profile 5-5′ (Fig. 3)

Fig. 11 Photos of the rainfall-triggered flood and landslides in Wanyuan County. (**a**–**b**) flood; (c–d) landslides

$$\phi = \arctan\left(\frac{Fs\sum W_i \sin\alpha_i - CL}{\sum W_i \cos\alpha_i}\right) \quad (2)$$

where C and ϕ are the cohesion and friction angle of the slip surface, respectively; Fs is the safety factor; W_i is the weight of the ith block; L is the length of the slip surface; and α_i is the dip angle of the slip surface of the ith block.

In practice, Chinese geologists have empirically concluded sound relationships among the safety factor and the deformation and failure characteristics of the landslide (Table 1). Two slip surfaces (S1 and S2) were identified based on the boreholes and exploratory trenches. The slip surface S1 is approximately in the shape of a circle, and the Sweden slice method is used in the stability evaluation of the slip surface S1. The Fs of the slip surface S1 using the Sweden slice method is calculated with the following equations:

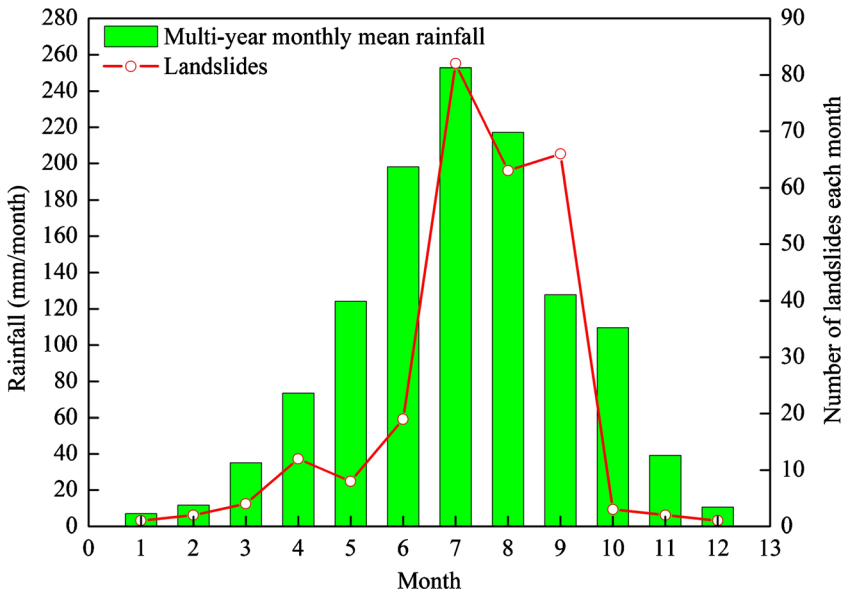

Fig. 12 The monthly distribution of the landslides and rainfall in the period 1985–2017 in Wanyuan County

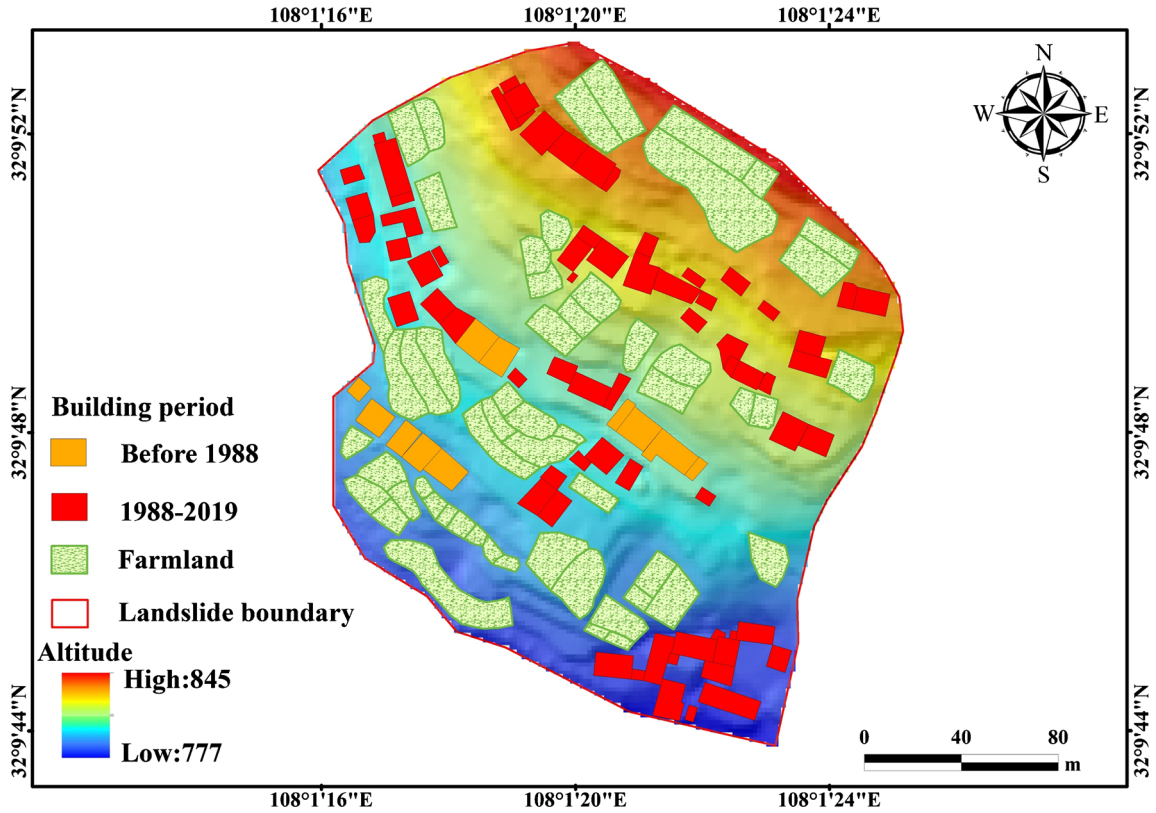

Fig. 13 Consistent human interventions in the landslide body

$$Fs = \frac{\sum((W_i((1-r_U)\cos\alpha_i - A\sin\alpha_i) - R_{D_i})\tan\phi_i + C_i L_i)}{\sum(W_i(\sin\alpha_i + A\cos\alpha_i) + T_{D_i})} \quad (3)$$

$$T_{D_i} = \gamma_W h_{i_W} L_i \sin\beta_i \cos(\alpha_i - \beta_i) \quad (4)$$

$$R_{D_i} = \gamma_W h_{i_W} L_i \sin\beta_i \sin(\alpha_i - \beta_i) \quad (5)$$

where C_i and ϕ_i are the shear strength parameters of the slip surface, respectively; A is the earthquake acceleration; T_{Di} and R_{Di} are the forces generated by the seepage pressure; L_i is the length of the slip surface of the ith block; r_U is the pore pressure ratio; h_{iW} is the groundwater level of the ith block; γ_W is the unit weight of water; and β_i is the groundwater flow direction of ith block.

The slip surface S2 is simplified as a polyline, and the transfer coefficient method is used to calculate the *Fs* of the slip surface S2. The *Fs* of the slip surface S2 using the transfer coefficient method can be calculated using the following equations:

Fig. 14 Damage of drainage ditch. **a** The tension crack of drainage ditch and **b** the dislocation near the furrow bank

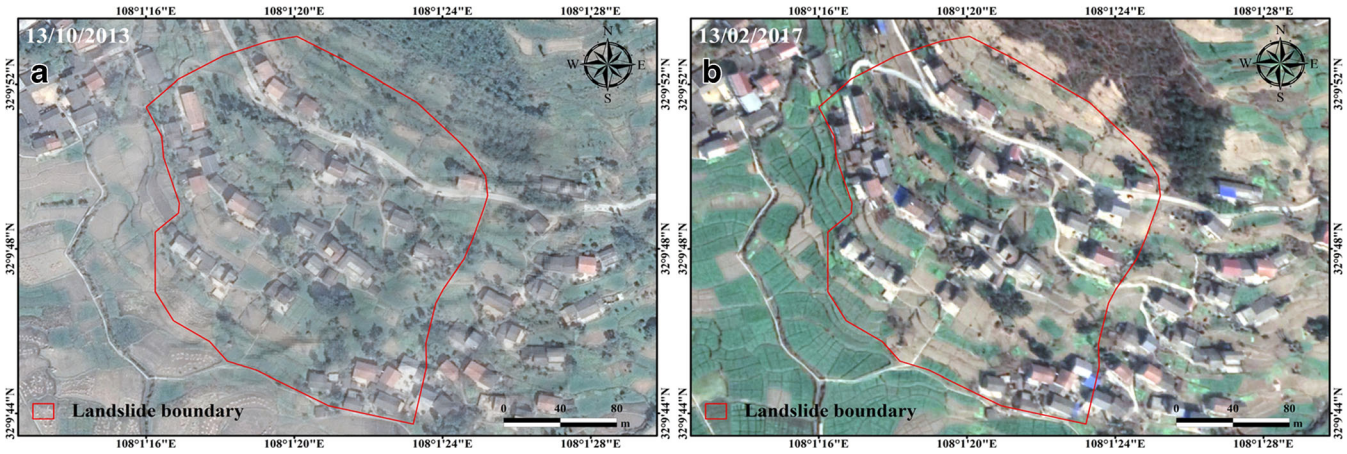

Fig. 15 Forest losses between 2013 and 2017. **a** Google Earth image taken on October 13, 2013. **b** Google Earth image taken on February 13, 2017

Table 1 Relationship between safety factor and developed stage (Luo et al. 2017)

Stage	Surface deformation	Maximal displacement of sliding plane	Status of sliding plane	Safety factor
Embryonic	Invisible	Millimeters	–	≥ 1.1
Creep	Deformation evidence at scarp and toe	Centimeters	At limit equilibrium state	1.0–1.1
Sliding	Main scarp subsidence and toe bulge	Decimeters-meters	Complete failure	0.95–1.0
Emplacement	Sedimentation, partial collapse	–	–	≥ 1.0

$$Fs = \frac{\sum_{i=1}^{n-1}\left(((W_i((1-r_U)\cos\alpha_i - A\sin\alpha_i) - R_{D_i}\cos\alpha_i)\tan\phi_i + C_iL_i)\prod_{j=i}^{n-1}\psi_j\right) + R_n}{\sum_{i=1}^{n-1}\left[(W_i(\sin\alpha_i + A\cos\alpha_i) + T_{D_i}\cos\alpha_i)\prod_{j=i}^{n-1}\psi_j\right] + T_n} \quad (6)$$

$$R_n = (W_n((1-r_U)\cos\alpha_n - A\sin\alpha_n) - R_{D_n})\tan\phi_n + C_nL_n \quad (7)$$

$$T_n = \left(W_n(\sin\alpha_n + A\cos\alpha_n) + T_{D_n}\right. \quad (8)$$

Table 2 Safety factors of the Linjiabang landslide under different scenarios

Sliding plane	Emergency mitigation measures	Scenarios	Safety factor	Stable state
S1	No	Normal	1.01	Basic stable
		Rainstorm	0.86	Unstable
		Earthquake	0.94	Unstable
	Yes	Normal	1.15	Basic stable
		Rainstorm	1.06	Basic stable
		Earthquake	1.11	Basic stable
S2	No	Normal	1.03	Basic stable
		Rainstorm	0.88	Unstable
		Earthquake	0.97	Unstable
	Yes	Normal	1.17	Basic stable
		Rainstorm	1.07	Basic stable
		Earthquake	1.12	Basic stable

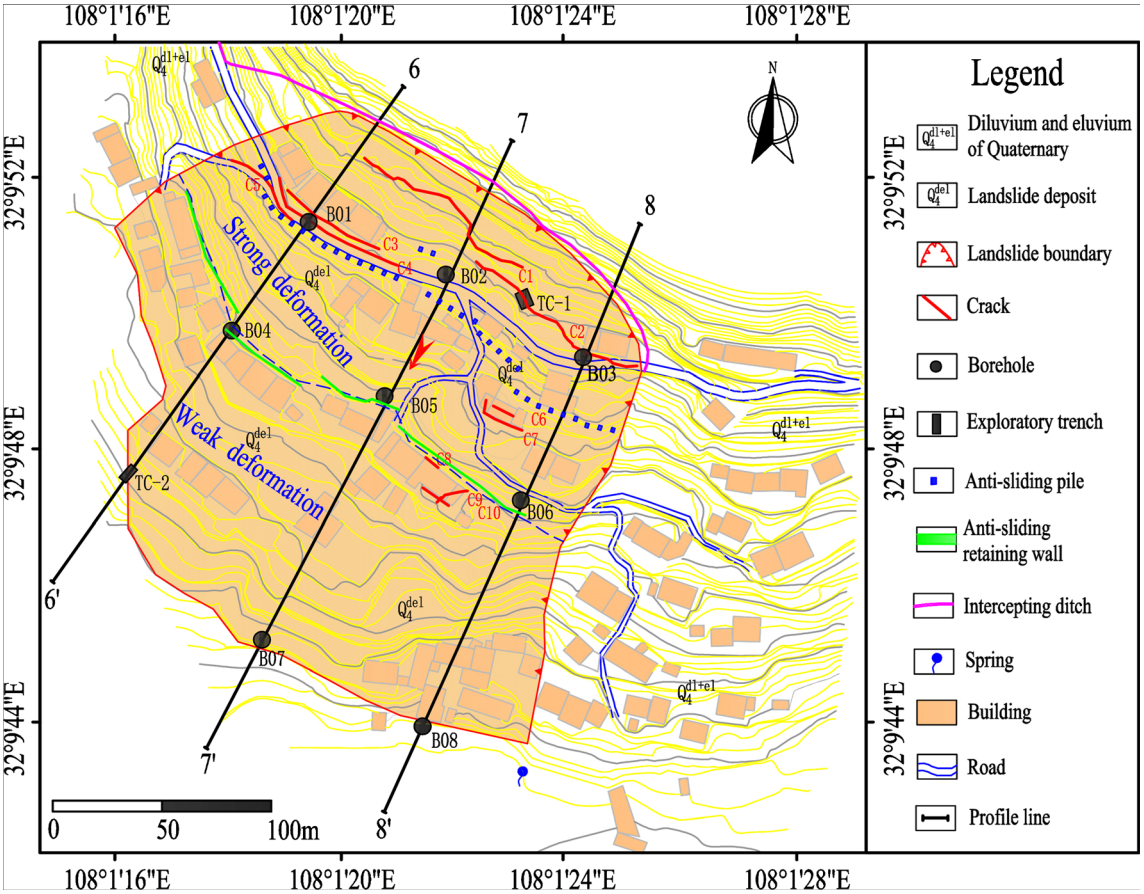

Fig. 16 Plan view of proposed engineering control measures to prevent landsliding

$$\prod_{j=i}^{n-1}\psi_j=\psi_i\psi_{i+1}\psi_{i+2}\ldots\psi_{n-1} \quad (9) \qquad \psi_j=\cos(\alpha_i-\alpha_{i+1})-\sin(\alpha_i-\alpha_{i+1})\tan\phi_{i+1} \quad (10)$$

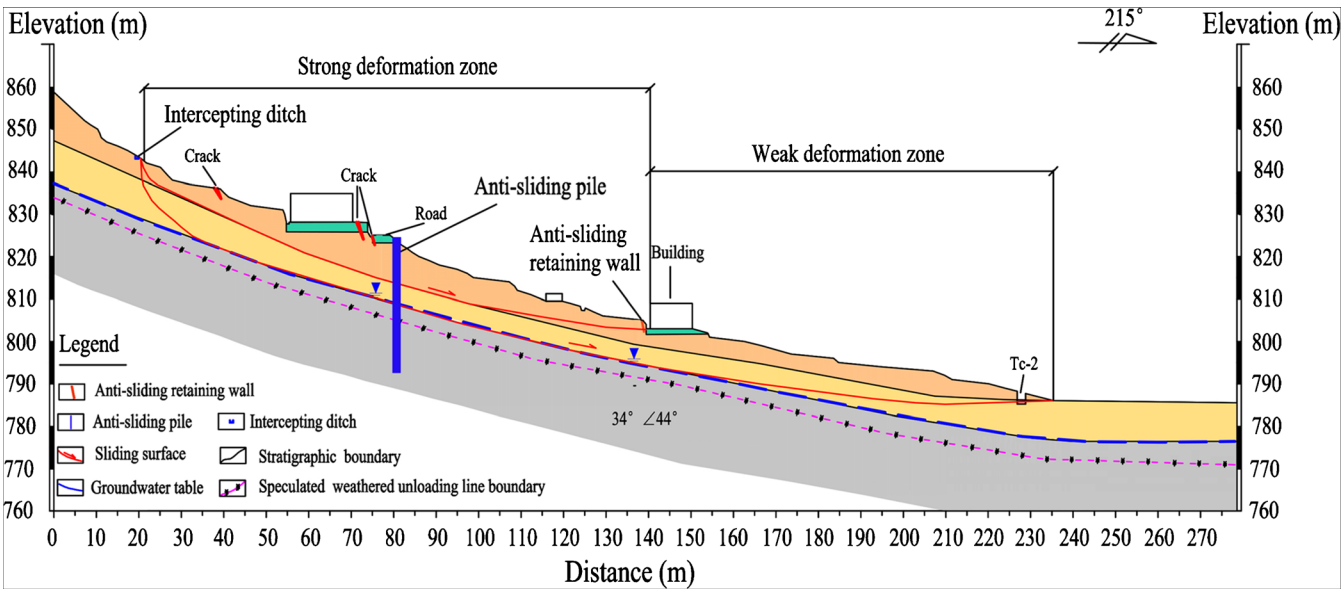

Fig. 17 Longitudinal geological profile 6-6′ (Fig. 16)

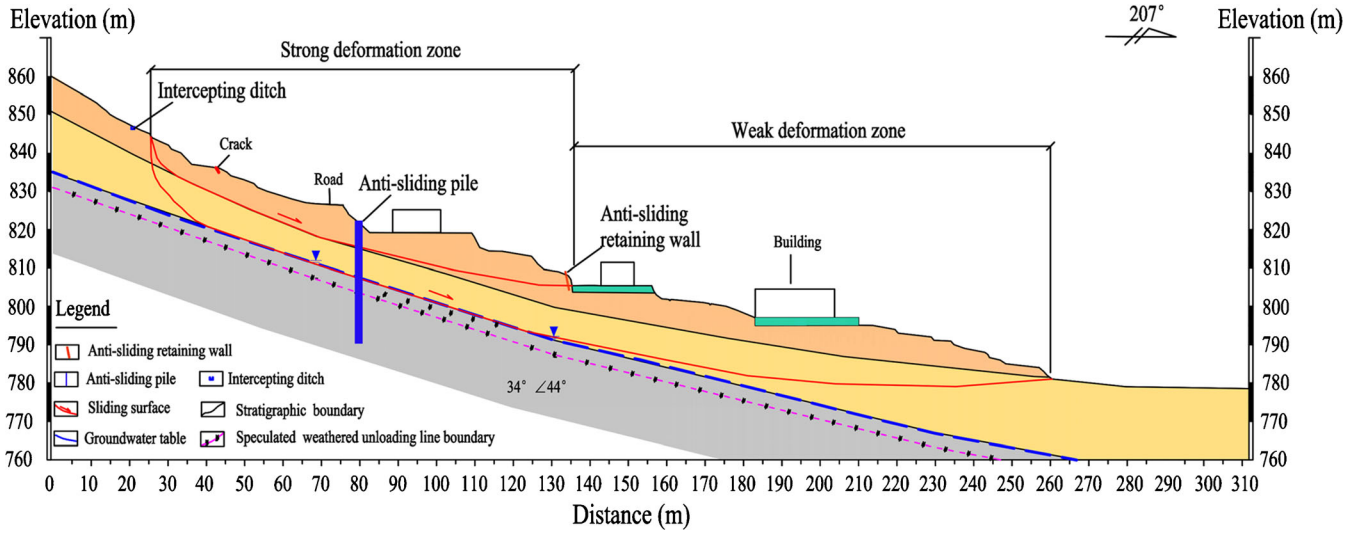

Fig. 18. Longitudinal geological profile 7-7′ (Fig. 16)

where ψ_j is the transfer coefficient of the ith block to the $(i + 1)$th block; $i = 1, 2, \ldots, n - 1$; and n is the total number of the soil blocks.

The safety factors of the Linjiabang landslide were calculated under different scenarios (Table 2), indicating that the landslide without stabilization work would become unstable under strong rainfall or earthquake conditions.

Proposed engineering control measures and some advice for the future

According to the landslide characteristics, the main engineering control measures include anti-sliding piles, an anti-sliding retaining wall, and intercepting ditch (Figs. 16, 17, 18, and 19). The anti-sliding piles and retaining wall provide resisting forces to reduce slope instability, and interception and drainage of water could improve the soil strength. The design calculations of the piles, retaining wall, and intercepting ditch were determined based on the advice of Wang et al. (2014). The total number of piles is 36, the section size is 1.5 × 2.0 m, and the piles have a length of 30–32 m (14.5–15.5 m length above the lower slip surface and 15.5–16.5 m length below the lower slip surface). The center distance between the two adjacent piles is 6.0 m. The design details of the anti-sliding piles are shown in Fig. 20. The weight of the 22-mm-diameter longitudinal bar is 2.98 kg per meter, the 28-mm-diameter longitudinal bar is 4.83 kg per meter, and the 32-mm-diameter longitudinal bar is 6.31 kg per meter. In the case of satisfying the slope stability, we optimized the design of the longitudinal bars based on the

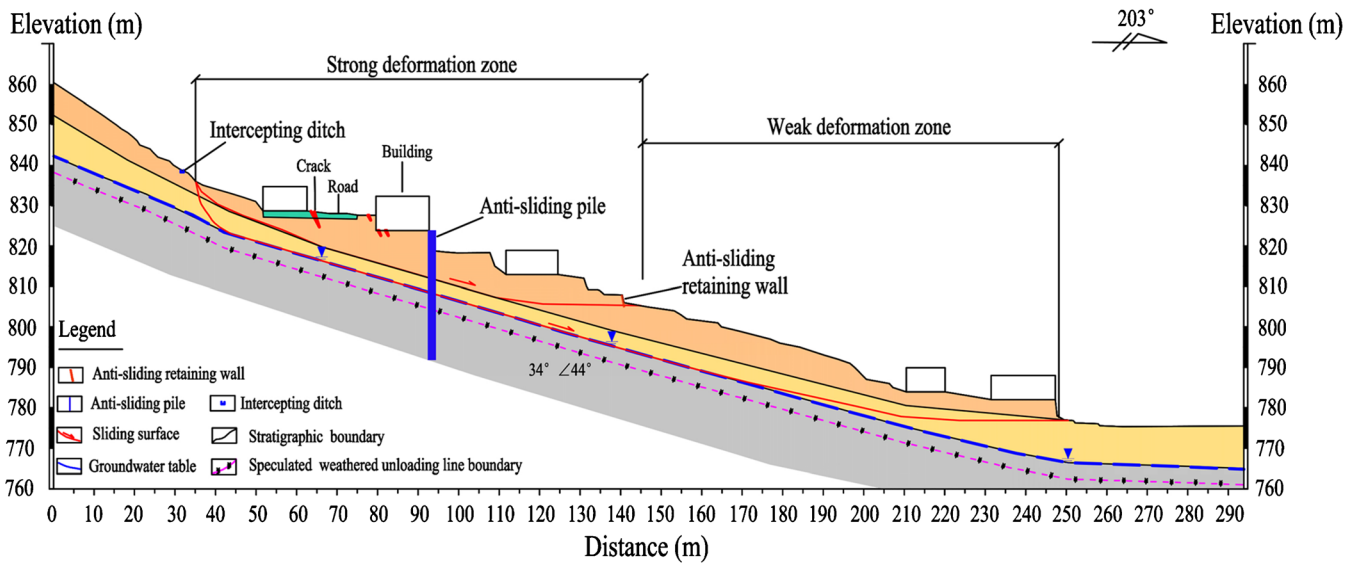

Fig. 19 Longitudinal geological profile 8-8′ (Fig. 16)

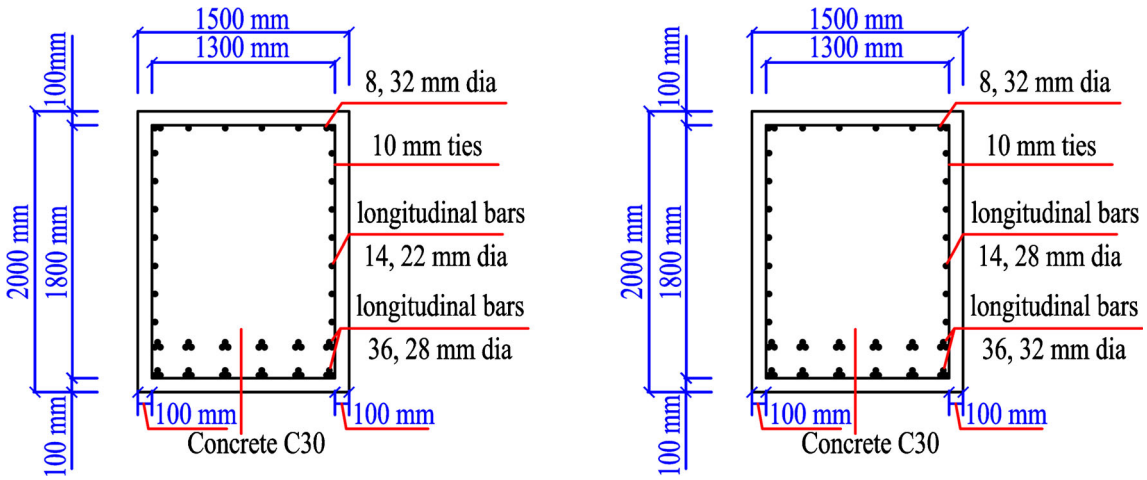

Fig. 20 Reinforced concrete pile design

principle of saving steel materials. Thus, the amount of the longitudinal bars per pile on the left part of the picture is less than the right part of the picture, saving about 2375.4–2533.8 kg of steel bars. The retaining wall is 3 to 5 m high, 216 m long, and has a width of 0.5 m at the crest. The section of the intercepting ditch is rectangular with a bottom width of 0.4 m, a depth of 0.3 m, a length of 330 m, a furrow bank that is 0.1 m wide, and a ditch base that is 0.15 m wide. The design details of the retaining wall and the intercepting ditch are shown in Fig. 21. The Linjiabang landslide with engineering control measures would become stable under rainstorm or earthquake conditions (Table 2).

Some landslide risk-reduction strategies can be expressed in some recommendations because the landslide mitigation measures have not been finished.

1. The landslide cracks should be covered with plastic sheets. This would prevent rainwater from seeping into the narrow cracks and restrain the increase in pore water pressure in the landslide.
2. Monitoring systems of the landslide should be implemented in the future. This should involve subsurface monitoring (such as groundwater levels and underground displacement) of the landslide using inclinometers. The inclinometers should be

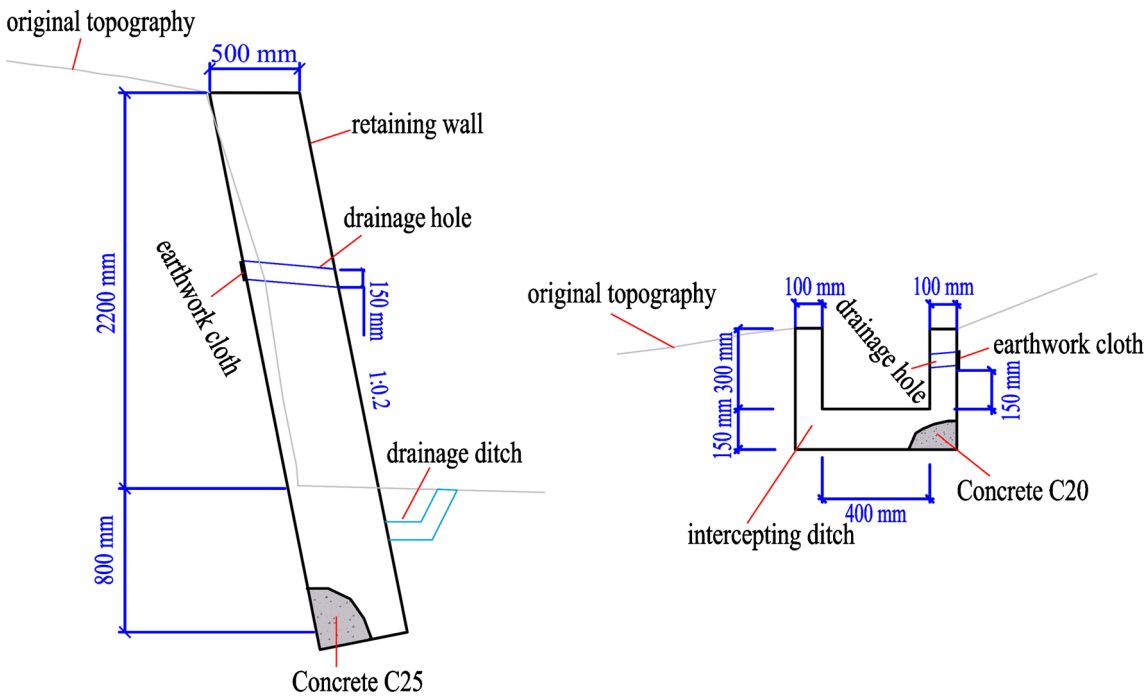

Fig. 21 The design details of the retaining wall and the intercepting ditch

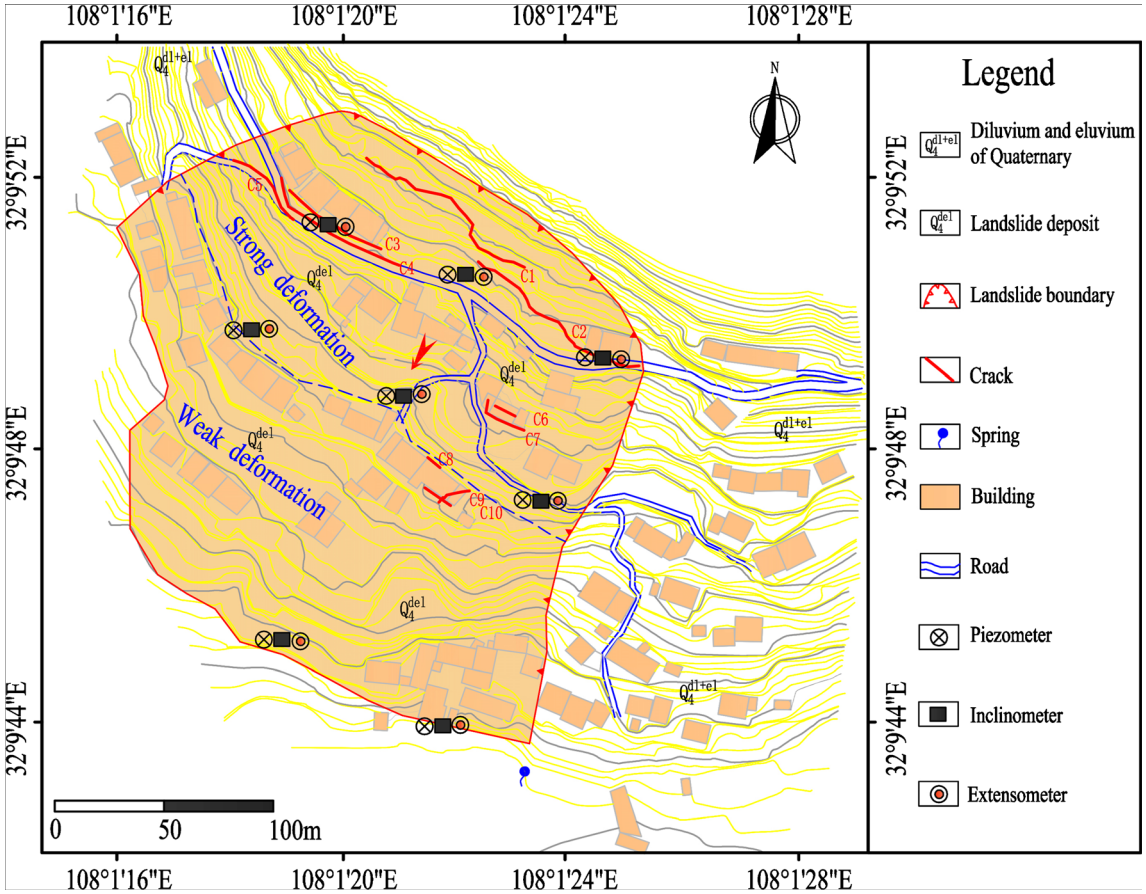

Fig. 22 Plan view of the proposed monitoring system

installed near the piezometers. Compared with underground displacement gages, extensometers can measure the relative surface displacements and are efficient for monitoring long-term, continuous movement. The proposed locations of these measures are shown in Fig. 22.

3. The appropriate land-use policies and regulations should be prepared based on the potential risks. It is necessary to take the potential geohazards into consideration in urban planning.

Conclusions

This paper reported that the Linjiabang landslide occurred on September 16, 2017, in Wanyuan County, Sichuan Province, China. Based on field investigations, boreholes, and exploratory trenches, we presented landslide features and possible triggering factors and then analysed landslide mitigation measures. The conclusions are as follows:

1. The Linjiabang landslide has been active for at least 34 years and is a typical slow-moving landslide in the hills area, with a total volume of 7.2×10^5 m^3. Two slip surfaces were determined based on the boreholes and exploratory trenches. The lower slip surface was the main sliding surface along the interface between bedrock and overlying deposits, and the upper slip surface was a secondary slip surface. The Linjiabang landslide could be divided into two deformation areas: the strong deformation area with abundant deformation (such as subsidence, tensile cracks, and bulges) and the weak deformation area with no obvious deformation but some tiny fissures formed during the rainy season.
2. Both the longer-term rainfall and anthropogenic activities (such as slope cutting for houses, land use changes, and deforestation) were considered to be the main triggering factors of the landslide.
3. At present, the landslide is unstable overall. Therefore, the main engineering measures, including anti-sliding piles, an anti-sliding retaining wall, and intercepting ditch, were implemented to control the continuous displacement of the landslide. However, the engineering measures have not yet been finalized, so some interim measures are required to effectively mitigate the landslide disaster. In addition, the effectiveness of the above measures should be further tested, and some efforts should be carried out for modeling the landslide by the physical-based model.

Funding informationThis study was supported by the National Nature Science Foundation of China (No. 41702311, 41601422).

References

Bromhead EN (1992) The stability of slopes. Blackie Academic and Professional, Great Britain

Đurić D, Mladenović A, Pešić-Georgiadis M, Marjanović M, Abolmasov B (2017) Using multiresolution and multitemporal satellite data for post-disaster landslide inventory in the Republic of Serbia. Landslides 14:1467–1482. https://doi.org/10.1007/s10346-017-0847-2

Gischig V, Preisig G, Eberhardt E (2016) Numerical investigation of seismically induced rock mass fatigue as a mechanism contributing to the progressive failure of deep-seated landslides. Rock Mech Rock Eng 49:2457–2478. https://doi.org/10.1007/s00603-015-0821-z

Hu G, Liu M, Chen N, Zhang X, Wu K, Khanal B, Han D (2019) Real-time evacuation and failure mechanism of a giant soil landslide on 19 July 2018 in Yanyuan County, Sichuan Province, China. Landslides 16:1177–1187. https://doi.org/10.1007/s10346-019-01175-x

Huang R, Jiang L, Shen X, Dong Z, Zhou Q, Yang B, Wang H (2019) An efficient method of monitoring slow-moving landslides with long-range terrestrial laser scanning: a case study of the Dashu landslide in the Three Gorges Reservoir Region, China. Landslides 16:839–855. https://doi.org/10.1007/s10346-018-1118-6

Lin F, Wu LZ, Huang RQ, Zhang H (2018) Formation and characteristics of the Xiaoba landslide in Fuquan, Guizhou, China. Landslides 15:669–681. https://doi.org/10.1007/s10346-017-0897-5

Luo G, Hu X, Bowman ET, Liang J (2017) Stability evaluation and prediction of the Dongla reactivated ancient landslide as well as emergency mitigation for the Dongla Bridge. Landslides 14:1403–1418. https://doi.org/10.1007/s10346-017-0796-9

Ma G, Hu X, Yin Y, Luo G, Pan Y (2018) Failure mechanisms and development of catastrophic rockslides triggered by precipitation and open-pit mining in Emei, Sichuan, China. Landslides 15:1401–1414. https://doi.org/10.1007/s10346-018-0981-5

Ma S, Xu C, Shao X, Zhang P, Liang X, Tian Y (2019) Geometric and kinematic features of a landslide in Mabian Sichuan, China, derived from UAV photography. Landslides 16:373–381. https://doi.org/10.1007/s10346-018-1104-z

Mendjel D, Messast S (2012) Development of limit equilibrium method as optimization in slope stability analysis. Struct Eng Mech 41:339–348. https://doi.org/10.12989/sem.2012.41.3.339

Samodra G, Hadmoko DS, Wicaksono GN, Adi IP, Yudinugroho M (2018) The March 25 and 29, 2016 landslide-induced debris flow at Clapar, Banjarnegara, Central Java. Landslides 15:985–993. https://doi.org/10.1007/s10346-018-0958-4

Shirzadi A, Shahabi H, Chapi K, Bui DT, Pham BT, Shahedi K, Ahmad BB (2017) A comparative study between popular statistical and machine learning methods for simulating volume of landslides. Catena 157:213–226. https://doi.org/10.1016/j.catena.2017.05.016

Song D, Che A, Zhu R, Ge X (2018) Dynamic response characteristics of a rock slope with discontinuous joints under the combined action of earthquakes and rapid water drawdown. Landslides 15(6):1109–1125. https://doi.org/10.1007/s10346-017-0932-6

Song D, Che A, Zhu R, Ge X (2019) Natural frequency characteristics of rock masses containing a complex geological structure and their effects on the dynamic stability of slopes. Rock Mech Rock Eng 52:1–17. https://doi.org/10.1007/s00603-019-01885-7

Wang B, Vardon PJ, Hicks MA (2016) Investigation of retrogressive and progressive slope failure mechanisms using the material point method. Comput Geotech 78:88–98. https://doi.org/10.1016/j.compgeo.2016.04.016

Wang J, Liang Y, Zhang H, Wu Y, Lin X (2014) A loess landslide induced by excavation and rainfall. Landslides 11:141–152. https://doi.org/10.1007/s10346-013-0418-0

Wei Z, Yin G, Wang JG, Wan L, Jin L (2012) Stability analysis and supporting system design of a high-steep cut soil slope on an ancient landslide during highway construction of Tehran–Chalus. Environ Earth Sci 67(6):1651–1662. https://xs.scihub.ltd/. https://doi.org/10.1007/s12665-012-1606-2

Xu L, Dai F, Chen J, Iqbal J, Qu Y (2014) Analysis of a progressive slope failure in the Xiangjiaba reservoir area, Southwest China. Landslides 11:55–66. https://doi.org/10.1007/s10346-012-0373-1

Yerro A, Pinyol NM, Alonso EE (2016) Internal progressive failure in deep-seated landslides. Rock Mech Rock Eng 49:2317–2332. https://doi.org/10.1007/s00603-015-0888-6

Zhang F, Huang X (2018) Trend and spatiotemporal distribution of fatal landslides triggered by non-seismic effects in China. Landslides 15:1663–1674. https://doi.org/10.1007/s10346-018-1007-z

Z. Chen · C. Hu
State Key Laboratory of Hydraulic and Mountain River Engineering, College of Water Resource and Hydropower,
Sichuan University,
Chengdu, 610065, China

D. Song (✉)
Department of Hydraulic Engineering, State Key Laboratory of Hydroscience and Engineering,
Tsinghua University,
Beijing, 100084, China
Email: Danqingsonglzu@163.com

Y. Ke
GEOPS, Univ. Paris-Sud, CNRS,
Université Paris-Saclay,
91405, Orsay, France